

## Article

# New Glycosalen–Manganese(III) Complexes and RCA<sub>120</sub> Hybrid Systems as Superoxide Dismutase/Catalase Mimetics

Valeria Lanza <sup>1</sup> and Graziella Vecchio <sup>2,\*</sup>

<sup>1</sup> Istituto di Cristallografia, Consiglio Nazionale delle Ricerche, Via Gaifami 18, 95125 Catania, Italy; valeria.lanza@cnr.it

<sup>2</sup> Dipartimento di Scienze Chimiche, Università di Catania, Viale A. Doria 6, 95125 Catania, Italy

\* Correspondence: gr.vecchio@unict.it

**Abstract:** Reactive oxygen species are implicated in several human diseases, including neurodegenerative disorders, cardiovascular dysfunction, inflammation, hereditary diseases, and ageing. Mn<sup>III</sup>–salen complexes are superoxide dismutase (SOD) and catalase (CAT) mimetics, which have shown beneficial effects in various models for oxidative stress. These properties make them well-suited as potential therapeutic agents for oxidative stress diseases. Here, we report the synthesis of the novel glycoconjugates of salen complex, EUK-108, with glucose and galactose. We found that the complexes showed a SOD-like activity higher than EUK-108, as well as peroxidase and catalase activities. We also investigated the conjugate activities in the presence of Ricinus communis agglutinin (RCA<sub>120</sub>) lectin. The hybrid protein–galactose–EUK-108 system showed an increased SOD-like activity similar to the native SOD1.

**Keywords:** carbohydrate; salen; manganese; SOD mimetics; EUK-108; EUK-8



**Citation:** Lanza, V.; Vecchio, G. New Glycosalen–Manganese(III) Complexes and RCA<sub>120</sub> Hybrid Systems as Superoxide Dismutase/Catalase Mimetics. *Biomimetics* **2023**, *8*, 447. <https://doi.org/10.3390/biomimetics8050447>

Academic Editor: Jose Luis Chiara

Received: 10 July 2023

Revised: 17 September 2023

Accepted: 19 September 2023

Published: 21 September 2023



**Copyright:** © 2023 by the authors. Licensee MDPI, Basel, Switzerland. This article is an open access article distributed under the terms and conditions of the Creative Commons Attribution (CC BY) license (<https://creativecommons.org/licenses/by/4.0/>).

## 1. Introduction

Oxidative stress occurs from the imbalance between radical species and antioxidant defences. It has been associated with various adverse health conditions, such as chronic inflammation, diabetes, cancer, neurodegenerative diseases (Parkinson’s disease, Alzheimer’s disease, ALS), and ageing [1,2].

Oxidative injury in cells is controlled and preserved through enzymatic and nonenzymatic antioxidant systems [3]. The superoxide dismutase (SOD), catalase (CAT), and peroxidase enzymes form the front line of defence against oxidative stress products. The main nonenzymatic antioxidants are vitamins (C and E), β-carotene, uric acid, and GSH.

In light of their impact on health, there has been an interest in targeting reactive oxygen species (ROS) in the development of redox medicine [4]. Many antioxidants and redox drugs have been administrated as therapeutic strategies for a variety of diseases [5]. The therapeutic potential of SOD enzymes has also been explored, and bovine CuZn–SOD preparations (Orgotein<sup>®</sup>) were administrated in the late 1970s to treat inflammatory diseases. Orgotein is only used as an anti-inflammatory drug in non-human animals [6]. MnSOD has also been investigated [7]. The therapeutical administration of SOD enzymes has several limitations, including the immunogenicity in the case of the SOD enzyme from non-human sources, the low intracellular uptake, short half-lives, administration route, and costs [8].

Low molecular weight complexes of redox metals (Fe, Cu, Mn) mimicking natural SOD enzymes have been widely reported [7,9,10]. SOD mimetics (SODm) would be potential therapeutics and useful probes to elucidate the physiopathologic role of intracellular superoxide radicals [10,11]. SODm have all been shown to positively affect the inflammatory state in lung epithelial cells in models of chronic obstructive pulmonary disease [12]. Mn<sup>II</sup> or Mn<sup>III</sup> complexes have been successfully studied as catalytic drugs among a variety of metal complexes, due to the low Fenton-based toxicity of manganese [13–15]. The Mn<sup>II</sup>

complexes of cyclic polyamines [15] aneN5 (1,4,7,10,13-pentaaza cyclopentadecane)-type ligands have been studied as SODm, and Imisopasem Manganese (M40403) and Avasopasem Manganese (M40419 or GC-4419) are the best systems in this family for diseases related to ROS dyshomeostasis. The GC-4419 is in a Phase 3 clinical trial to reduce side effects from anticancer therapy [16,17]. In 2020 Galera Therapeutics Inc. announced the phase II clinical trial with GC4419 for critical illness due to COVID-19 [18].

The Mn<sup>II</sup> complexes of polyamine (salan-type) ligands have also been investigated as SOD mimetics [19]. The salan ligands have also been functionalized with cell-penetrating peptides to improve their cell uptake and antioxidant activity [19]. Other families of SODm include the Mn<sup>III</sup> complexes of porphyrin- and Mn<sup>III</sup>-salen (H<sub>2</sub>salen = N,N'-bis(salicylidene)ethylenediamine)-type complexes [20,21]. The Mn<sup>III</sup> complexes of a variety of porphyrins have been widely studied [14,15,22,23].

Mn<sup>III</sup>-salen derivatives have been developing as combined SOD/CAT mimetics mainly by Eukarion Company [24–26]. Eukarion (EUK)-8 (or EUK-108 when the ligand is CH<sub>3</sub>COO<sup>-</sup> instead of Cl<sup>-</sup>) and EUK-134 (or EUK-113 when the ligand is CH<sub>3</sub>COO<sup>-</sup> instead of Cl<sup>-</sup>) are the prototype molecules of this family of complexes and have been tested in several pathological conditions [5,27,28]. Currently, EUK-134 is a component of numerous anti-ageing skincare products for its antioxidant properties. Various salen-type complexes have been studied recently in in vitro and in vivo animal models of diseases closely related to oxidative stress, such as neurodegenerative diseases and cancer [25,29–32].

Based on the interest in salen derivatives [7,24,28,29,33,34], herein, we report the synthesis of two new Mn<sup>III</sup> salen glycoconjugates. In particular, we conjugated an N,N'-bis(salicylidene) ethylenediamine derivative with glucose or galactose to synthesize EUK-108-analogous molecules (Figure 1).

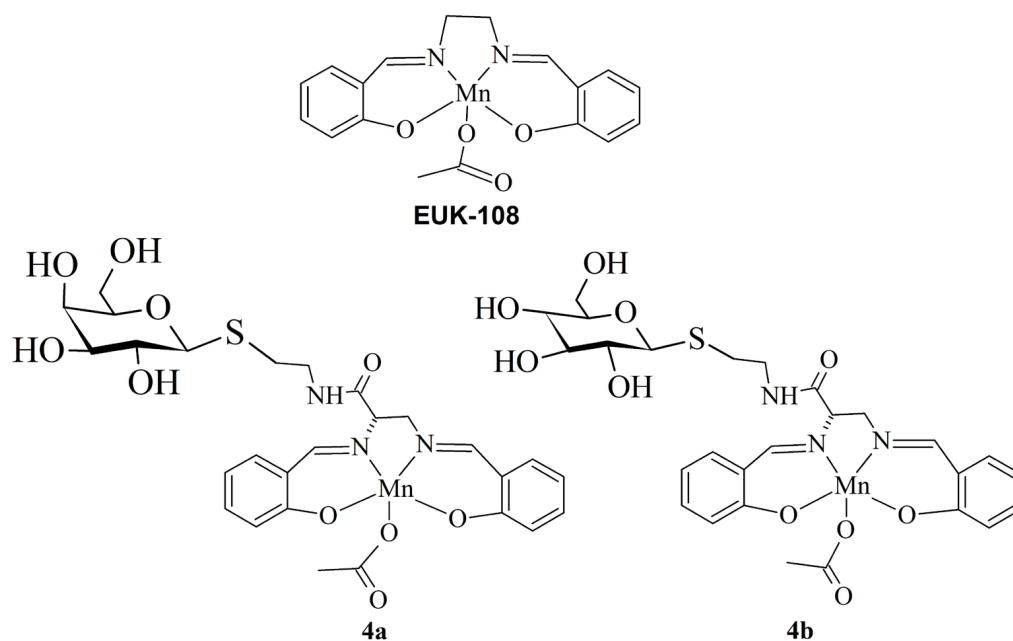


**Figure 1.** Structures of EUK-108 and Glycoconjugates synthesized in this study.

We exploited the new features introduced by sugar moiety, such as the binding with specific lectins [35]. Ricinus communis agglutinin I (RCA<sub>120</sub>, RCA I) is a glycoprotein composed of two A and two B units linked by a disulfide bond. Subunit A is the catalytic unit and confers toxicity to the protein, while chain B binds carbohydrate chains with non-reducing terminal galactose residues [36]. RCA<sub>120</sub> has low toxicity compared to the homolog ricin protein.

In the last few years, metal complexes have been caged in protein scaffolds to form artificial metalloenzymes, also called hybrids, and engineer new reactions [37–40]. Many

anchoring strategies have been explored to build new artificial metalloenzymes. The properties of the scaffold protein can modulate the catalytic activity of the metal complex that acts as an artificial prosthetic group. The protein moiety provides a unique microenvironment (chirality, dielectric coefficient) and can improve solubility and substrate accessibility [37–40]. Some examples of the non-covalent strategy exploit the affinity of the metal complex for the protein, such as the streptavidin–biotin technology, which is applied in vivo for catalyzing abiotic reactions [41].

We synthesized non-covalent conjugates of RCA<sub>120</sub> with galactose–salen conjugate **4a**. We investigated the SOD-like, peroxidase, and catalase activities of the metal complexes and the RCA<sub>120</sub>–glycosalen complexes.

The hybrid protein–galactose–salen system showed an increased SOD-like activity.

## 2. Materials and Methods

### 2.1. Material

Anhydrous DMF, anhydrous methanol, acetobromo- $\alpha$ -D-galactose, acetobromo- $\alpha$ -D-glucose, N $\alpha$ , N $\beta$ -Di-Boc-L-2,3-diaminopropionic acid (dicyclohexylamine salt) (DAPBoc), cysteamine (2-mercaptoethylamine, mea), o-(benzotriazole-1-yl)-N,N,N',N'-bis(tetramethylene)O-(1H-benzotriazol-1-yl)-N,N,N',N'-tetramethyluronium tetrafluoroborate (TBTU), 1-hydroxybenzotriazole (HOBT), and lectin from *Ricinus communis* (RCA<sub>120</sub>) were purchased from Sigma-Aldrich and were used without any purification. CM Sephadex C-25 (Sigma) (NH<sub>4</sub><sup>+</sup> form) and DEAE-Sephadex A-25 (HCO<sub>3</sub><sup>-</sup> form) were used for ion exchange chromatography. Ultra-pure water (Milli-Q Element, Millipore, Italy) was used for all the experiments. Thin layer chromatography (TLC) was carried out on silica gel plates (Polygram SIL G/UV254 0.2 mm Macherey-negel). Glycosidic derivatives were detected on TLC using UV or the anisaldehyde test.

EUK-108 was synthesized as reported elsewhere [42].

### 2.2. Synthesis of Salen Ligands and Mn<sup>III</sup> Complexes

#### 2.2.1. Synthesis of 1-deoxy-1[(S-cysteamine)]- $\beta$ -galactose (**1a**) and of 1-deoxy-1[(S-cysteamine)]- $\beta$ -glucose (**1b**)

Mea (1.9 g, 24.6 mmol) and sodium methanolate (24.6 mmol) in water (2 mL) were added to a solution of  $\alpha$ -D-acetobromo-galactose (2.42 g, 5.9 mmol) in DMF (2 mL). The reaction was carried out at 70 °C under stirring and nitrogen. After 3h, the solvent was evaporated. The product was obtained through the hydrolysis of acetyl groups in NaOH (1%) for 2h. The product was purified through reverse-phase RP8 column chromatography, and eluted using a NH<sub>4</sub>Cl solution (0.1 M). The appropriate fractions were collected and evaporated (R<sub>f</sub> = 0.2, PrOH/H<sub>2</sub>O/AcOEt/NH<sub>3</sub>, 4:3:2:1). The solid residue was further purified by a CM Sephadex C-25 column (20 × 60 mm, NH<sub>4</sub><sup>+</sup> form) eluted using water and then a linear gradient of NH<sub>4</sub>HCO<sub>3</sub> solution (400 mL) 0 → 0.3 M. Product **1a** was obtained, with a yield of 30%. R<sub>f</sub> = 0.42 (PrOH/H<sub>2</sub>O/AcOEt/NH<sub>3</sub> 4:3:2:1).

ESI-MS:  $m/z$  = 240.1 (**1a** + H)<sup>+</sup>

<sup>1</sup>H NMR (D<sub>2</sub>O, 500 MHz)  $\delta$ (ppm): 4.37 (1H, d, J<sub>H1,H2</sub> = 10.0 Hz, H-1 of Gal); 3.86 (1H, d, J<sub>H3,H4</sub> = 4.0 Hz, H-4 of Gal); 3.67–3.56 (3H, m, H-5, H-6<sub>a</sub>, H-6<sub>b</sub> of Gal); 3.54 (1H, dd, J<sub>H3,H4</sub> = 4.0 Hz, J<sub>H2,H3</sub> = 10.0 Hz, H-3 of Gal); 3.46 (1H, t, J<sub>H1,H2</sub> = 10.0 Hz, H-2 of Gal); 2.80 (2H, m, CH<sub>2</sub> in  $\alpha$  to NH<sub>2</sub>); and 2.75 (m, 2H, CH<sub>2</sub> in  $\beta$  to NH<sub>2</sub>).

The same procedure given for **1a** was followed to synthesize **1b**), starting from  $\alpha$ -D-acetobromo-glucose. The yield was 35%. R<sub>f</sub> = 0.42 (PrOH/H<sub>2</sub>O/AcOEt/NH<sub>3</sub> 4:3:2:1).

ESI-MS  $m/z$  = 240.0 (**1b** + H)<sup>+</sup>

<sup>1</sup>H NMR (D<sub>2</sub>O, 500 MHz)  $\delta$ (ppm): 4.44 (1H, d, J<sub>H1,H2</sub> = 10.0 Hz, H-1 of Glc); 3.80 (1H, dd, J<sub>H5,H6</sub> = 9.0 Hz, J<sub>H6,H6'</sub> = 12.0 Hz, H-6<sub>a</sub> of Glc); 3.60 (1H, dd, J<sub>H6a,H6b</sub> = 12.0 Hz, H-6<sub>b</sub> of Glc); 3.38 (2H, m, H-3, H-5 of Glc); 3.31 (1H, t, J<sub>H4,H5</sub> = 9.0 Hz, H-4 of Glc); 3.23(1H, t, J<sub>H1,H2</sub> = 10.0 Hz, H-2 of Glc); 2.83 (2H, m, CH<sub>2</sub> in  $\alpha$  to NH<sub>2</sub>); and 2.73 (2H, m, CH<sub>2</sub> in  $\beta$  to NH<sub>2</sub>).

### 2.2.2. Synthesis of 1-deoxy-1[(S-cysteamidopropyl(1,2-diamino)]-β-galactose] **2a** and 1-deoxy-1[(S-cysteamidopropyl(1,2-diamino)]-β-glucose] **2b**

DAPBoc (250 mg, 0.82 mmol), TBTU (315mg, 0.82 mmol), and HOBT (111 mg, 0.82 mmol) in dry DMF (30 mL) were stirred under nitrogen at 25 °C. After 15 min, **1a** was added (200 mg, 0.82 mmol) to the solution. The reaction was stopped when the reagents disappeared in TLC (PrOH/H<sub>2</sub>O/AcOEt/NH<sub>3</sub>, 5:2:1:1). DMF was evaporated and the solid was purified through a reverse-phase C-8 column with a gradient of H<sub>2</sub>O/acetone (0→50%). The Boc group was removed with CF<sub>3</sub>COOH for 1h. CF<sub>3</sub>COOH was evaporated and the product was passed through a DEAE-Sephadex A-25, using water as the eluent. R<sub>f</sub> = 0.31 (PrOH/H<sub>2</sub>O/AcOEt/NH<sub>3</sub>,5:2:2:2); and the yield was 40%.

ESI-MS *m/z* = 326.4 (**2a** + H)<sup>+</sup>

<sup>1</sup>H NMR (D<sub>2</sub>O, 500 MHz) δ(ppm): 4.40 (1H, d, J<sub>H1,H2</sub> = 10.0 Hz H-1 of Gal); 3.88 (1H, d, J<sub>H3,H4</sub> = 3.0 Hz, H-4 of Gal); 3.70–3.58 (3H, m, H-5, H-6<sub>a</sub>, H-6<sub>b</sub> of Gal); 3.55 (1H, dd, J<sub>H2,H3</sub> = 10.0 Hz, J<sub>H3,H4</sub> = 3.0 Hz, H-3 of Gal); 3.46 (1H, t, J<sub>H1,H2</sub> = 10.0 Hz, H-2 of Gal); 3.40 (3H, m, CH<sub>2</sub> in b to S, CH of DAP); 2.85 (1H, m, CH<sub>2</sub> of DAP); and 2.78 (4H, m, CH<sub>2</sub> in a to S and CH<sub>2</sub> of DAP).

**2b** was synthesized as reported for **2a**

ESI-MS *m/z* = 326.6 (**2b** + H)<sup>+</sup>

<sup>1</sup>H NMR (D<sub>2</sub>O, 500 MHz) δ (ppm): 4.36 (1H, d, J<sub>H1,H2</sub> = 10.0 Hz H-1 of Glu); 3.84 (1H, d, J<sub>H3,H4</sub> = 10.0 Hz H-4 of Glc); 3.68–3.56 (3H, m, H-5, H-6<sub>a</sub>, H-6<sub>b</sub> of Glc); 3.53 (1H, dd, J<sub>H2,H3</sub> = 4.0 Hz, J<sub>H3,H4</sub> = 10.0 Hz, H-3 of Glc); 3.46 (H, t, J<sub>H-H</sub> = 10.0 Hz, H-2 of Glc); 3.38 (3H, m, CH<sub>2</sub> in β to S, CH of DAP); 2.82 (2H, m, CH<sub>2</sub> of DAP); and 2.75 (4H, m, CH<sub>2</sub> in α to S).

### 2.2.3. Synthesis of 1-deoxy-1[(S-cysteamidopropyl(1,2-diamino)N,N'-bis(salicylidene)]-β-galactose] **3a**

**2a** (50 mg, 1.5 mmol) was dissolved in anhydrous methanol (5 mL) and a stoichiometric amount of salicylaldehyde (12.5 mL, 3.0 mmol) was added under stirring at 25 °C. A yellow solid was formed. After 6 h, the solvent was evaporated under vacuum and the solid obtained was washed with hexane/acetone (1:1). The yield was 88%.

ESI-MS *m/z* = 534.5 (**3a** + H)<sup>+</sup>

<sup>1</sup>H NMR (CD<sub>3</sub>OD, 500 MHz) δ (ppm): 8.54 (s; 1H, m, imine H); 8.45(s; 1H, s, imine H); 7.32 (4H, m, H-6 and H-3); 6.82–6.83 (4H, m, H-4 and H-5); 4.33 (1H, d, J<sub>XY</sub> = 6.0 Hz CH in α to O=C); 4.31 (1H, d, J<sub>1,2</sub> = 9.70 Hz Gal H-1 and CH); 4.15 (2H, m, CHa in β to O=C-NH); 4.05 (2H, m, CHb in β to O=C-NH); 3.84 (1H, d, J<sub>H3,H4</sub> = 5.0 Hz, Gal H-4); 3.75 (1H, m, Gal H-5); 3.46 (1H, dd, J<sub>H2,H3</sub> = 11.0 Hz, J<sub>H3,H4</sub> = 5.0 Hz, Gal H-3); 3.57–3.48 (3H, m, Gal H-6, H-6', H-2); 3.42 (2H, m, CH<sub>2</sub> in α to -NH-C=O); 2.89 (2H, m, CHa in β to -NH-C=O); and 2.77 (2H, m, CHb in β to O=C-NH). The glucose–salen conjugate **3b** was synthesized as reported for **3a**.

ESI-MS *m/z* = 534.0 (**3b** + H)<sup>+</sup>

<sup>1</sup>H NMR (CD<sub>3</sub>OD, 500 MHz) δ(ppm): 8.53 (1H, s, imine H); 8.45 (1H, s, imine H); 7.43–7.20 (4H, m, H-6 and H-3); 6.97–6.82 (4H, m, H-4 and H-5); 4.36 (1H, d, J<sub>H1,H2</sub> = 9.7 Hz, Glc H-1); 4.33 (1H, m, CH in α O=C-NH); 4.14 (2H, m, CHa in β to O=C-NH); 4.05 (2H, m, CHb in β to O=C-NH); 3.84 (1H, d, J<sub>H3,H4</sub> = 5.0 Hz, Glc H-4); 3.84 (1H, d, J<sub>3,4</sub> = 12.0 Hz, Glc H-6); 3.61–3.45 (5H, m, Glc H-5, H-4, H-6', CH<sub>2</sub> in α to -NH-C=O); 3.26 (1H, m, Glc H-3); 3.19 (1H, t, J<sub>H1,H2</sub> = 10.0 Hz, Glc H-2); 2.88 (2H, m, CHa in β to -NH-C=O); and 2.72 (2H, m, 2H, CHb in β to O=C-NH).

### 2.2.4. Synthesis of Manganese(III) Complexes of **3a** and **3b**

**3a** (115 mg, 0.086 mmol) and NaOH (0.172 mmol, methanolic solution) were dissolved in anhydrous methanol (5 mL). Mn(CH<sub>3</sub>COO)<sub>2</sub> (0.086 mmol) was added to the solution under stirring. The yellow solution turned brown and the reaction mixture was refluxed. After 3 h, the precipitate was filtered off and washed with acetone. The solid was further purified through precipitation from a water and acetone solution.

The yield was 90%.

**4a**: ESI-MS  $m/z = 586.2$  [**4a**-Ac]<sup>+</sup>

**4b** was synthesized as reported for **4a**.

**4b**: ESI-MS  $m/z = 586.0$  [**4b**-Ac]<sup>+</sup>

### 2.2.5. Preparation of Hybrid Mn<sup>III</sup> and RCA<sub>120</sub> System

**4a**- or **4b**-RCA<sub>120</sub> adducts were prepared by incubating equimolar amounts of RCA<sub>120</sub> lectin and Mn complex for 10 min in the buffer solution, at 25 °C.

### 2.3. Instrumentation

The NMR spectra were recorded at 25 °C with a Varian Inova 500 spectrometer. The <sup>1</sup>H NMR spectra were acquired using standard Varian library pulse programs. The 2D spectra (COSY, TOCSY, HSQC) were acquired using 1K data points, 256 increments, and a relaxation delay of 1.5 s.

The mass spectra were recorded with a Mariner Perseptive Biosystem ESI-MS.

The UV-visible spectra were recorded with an Agilent 8452A diode array spectrophotometer. The CD spectra were performed on a JASCO model J-810 spectropolarimeter.

The **4a**, **4b**, and EUK-108 stock solutions were prepared in EtOH/water (1:1). The final EtOH concentration did not exceed 5% and did not affect the measurements. The spectra of freshly prepared solutions were recorded at 25 °C.

### 2.4. Superoxide Dismutase Assay

The SOD-like activity was determined using the indirect method [43]. Superoxide anion was generated by the xanthine/xanthine oxidase system and spectrophotometrically detected by monitoring the nitro blue tetrazolium (NBT) reduction to formazan at 560 nm, for 600 s.

The amount of xanthine oxidase required to produce a  $\Delta A_{560} \text{ nm/min} = 0.024$  was added to 2 mL of the reaction mixture (NBT 250  $\mu\text{M}$ , xanthine 50  $\mu\text{M}$ , phosphate buffer 0.010 M, pH 7.4), as reported elsewhere [44]. The  $\Delta A_{560} = 0.024 \text{ nm/min}$  corresponds to the 1.1 mM/min  $\text{O}_2$  production rate. The NBT reduction rate was also measured in the presence of the Mn<sup>III</sup> complexes (concentration ranging from 10<sup>-5</sup> to 10<sup>-8</sup> M). All measurements were carried out at 25 °C under stirring. In separate experiments, urate production was spectrophotometrically monitored at 295 nm to exclude the inhibition of xanthine oxidase activity in the presence of Mn<sup>III</sup> complexes or RCA<sub>120</sub>.

The I<sub>50</sub> value (the concentration of metal complex required to inhibit 50% of NBT reduction) was determined.

### 2.5. Catalase Activity Assay

The catalase activity was determined as reported elsewhere [34]. An H<sub>2</sub>O<sub>2</sub> solution (30 mM) was incubated at 25 °C with the Mn<sup>III</sup> complex (concentration ranging from 10<sup>-5</sup> to 10<sup>-6</sup> M) in 0.010 M phosphate buffer (pH 7.4).

ABTS (2,2-azino-bis(3-ethylbenzothiazoline-6-sulfonic acid) (50 mM) and horseradish peroxidase (1.3 mg/mL) were added after 50 min. The absorbance at 735 nm was measured after 5 min, and the amount of H<sub>2</sub>O<sub>2</sub> consumed per min per mmole from the compound was determined.

### 2.6. Peroxidase Activity Assay

The peroxidase activity of **4a**, **4b**, and EUK-108 compounds was assayed by monitoring spectrophotometrically the H<sub>2</sub>O<sub>2</sub>-dependent oxidation of ABTS [45]. The ABTS (0.2 mM), Mn<sup>III</sup> complex (10 mM), and H<sub>2</sub>O<sub>2</sub> (0.5 mM) in phosphate buffer (50 mM, pH 7.4) were incubated at 25 °C.

ABTS oxidation was monitored at 735 nm ( $\epsilon_{\text{ABTS}^+} = 15,000$ ) where the metal complexes did not show any absorption. No oxidation reaction of ABTS with the complexes was observed in the assay condition.

### 3. Results and Discussion

#### 3.1. The Ligands

**4a** and **4b** were synthesized from sugar amino-derivatives via the multistep procedure reported in Figure 2. The anomerically pure **1a** and **1b** were obtained in good yield through a nucleophilic substitution reaction between  $\alpha$ -D-acetobromo-glycoside and cysteamine in water at basic pH. The amino group of **1a** and **1b** was linked to DAPBoc through a condensation reaction, and the products were purified using reverse-phase chromatography.

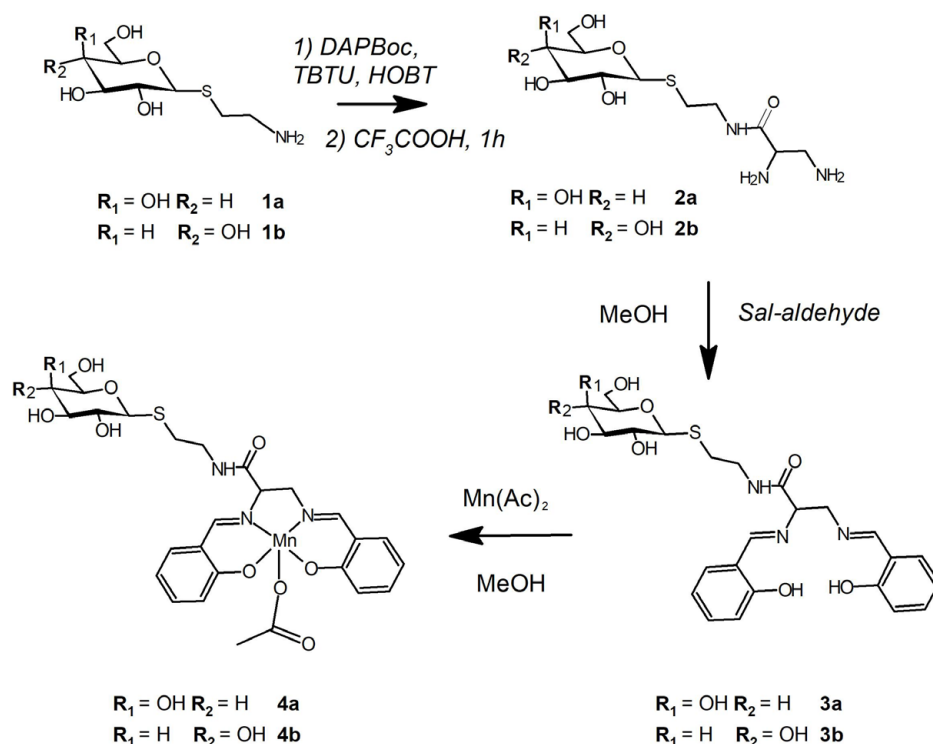


**Figure 2.** Synthesis scheme of **4a** and **4b**.

After removing the Boc-protecting groups through acid hydrolysis, the derivatives **2a** and **2b** were obtained and isolated through ionic-exchange chromatography. **3a** and **3b** were synthesized from **2a** and **2b** and sal-aldehyde at 25 °C in anhydrous methanol.

The NMR and ESI-MS spectra confirmed the identity of the products and intermediates (Figure S1–S13). In the  $^1\text{H}$  NMR spectrum of **1a** and **1b**, the signals of the sugar unit and the ethylenic chain were present. The chemical shift of the H-1 signal and the coupling constant values (10.0 Hz) confirmed the  $\beta$ -configuration of the anomeric carbon of the sugar residue. In the  $^1\text{H}$  NMR spectra of **2a**, the signals of the galactose protons were assigned using the COSY and TOCSY spectra. The protons of the cysteamine moiety resonated at 3.50 ppm and at 2.78 ppm, while the protons of the ABX system of the propionyl chain resonated at 3.40 ppm (X), 2.83 and 2.80 ppm (A, B). A similar trend was found in the **2b** spectrum.

In the  $^1\text{H}$  NMR spectra of **3a**, the imino protons appeared at 8.60 and 8.49 ppm. The signal at 8.60 ppm was assigned to the imino group  $\alpha$  to the amido group. The chemical shifts of the protons of the two benzene rings also resonated differently. The signals of the ABX system of the diamino-propionyl chain were evident in the spectra. The spectra of **3b** were similar to the spectra of **3a**.

#### 3.2. The Manganese(III) Complexes

The  $\text{Mn}^{\text{III}}$  complexes **4a** and **4b** were synthesized, as reported for salen complexes [46], at 25 °C and were isolated by adding acetone to the reaction mixture. The UV–Vis spectra of **4a** and **4b** were not significantly different from that of the parent salen complex EUK-108. In the spectra, there were the typical transitions at 323 nm, due to  $\pi \rightarrow \pi^*$  C=N groups

and at 388 nm, due to LMCT, suggesting the same coordination environment of the Mn<sup>III</sup> compared to EUK-108. In the ESI mass spectra (Figure S13), a leading peak corresponded to the complex species [Mn<sup>III</sup> complex]<sup>+</sup> (**4a** or **4b** without CH<sub>3</sub>COO<sup>-</sup> ligand).

### 3.3. SOD-like Activity

The reaction of **4a** and **4b** with the superoxide anion was determined by competition kinetic experiments with NBT being used as the target molecule [47,48]. Plotting  $V_0/V_{cat-1}$  versus the complex concentration produced a straight line with a slope  $k_{cat}/k_{NBT}[NBT]$  [49] (Figure S14), where  $V_0$  was the NBT reduction rate  $V_{cat}$  was the NBT reduction rate in the presence of the investigated complex, and  $k_{NBT}$  was  $5.88 \times 10^4 \text{ M}^{-1}\text{s}^{-1}$  [43,50]. The  $I_{50}$  and  $k_{cat}$  values are reported in Table I. **4a** and **4b** showed good SOD-like activity, and their  $I_{50}$  values were about ten times lower than that of EUK-108. The  $I_{50}$  values were similar to those reported for the EUK-108–cyclodextrin conjugate [44]. The effect of the modification of the salen–diamine bridge on catalytic activity has been explored in a few cases [26,45,51]. In the case of the cyclodextrin derivatives previously studied, we hypothesized the role of the hydrophobic cavity and/or OH groups in order to explain the improved SOD-like activity. The results on monosaccharide conjugates may suggest the prominent role of OH groups in improving the SOD-like activity of the catalytic center. Molecular modelling suggests that, in **4a** and **4b**, the sugar side-chain may bend toward the catalytic center (Figure 3), which could improve the SOD-like activity.

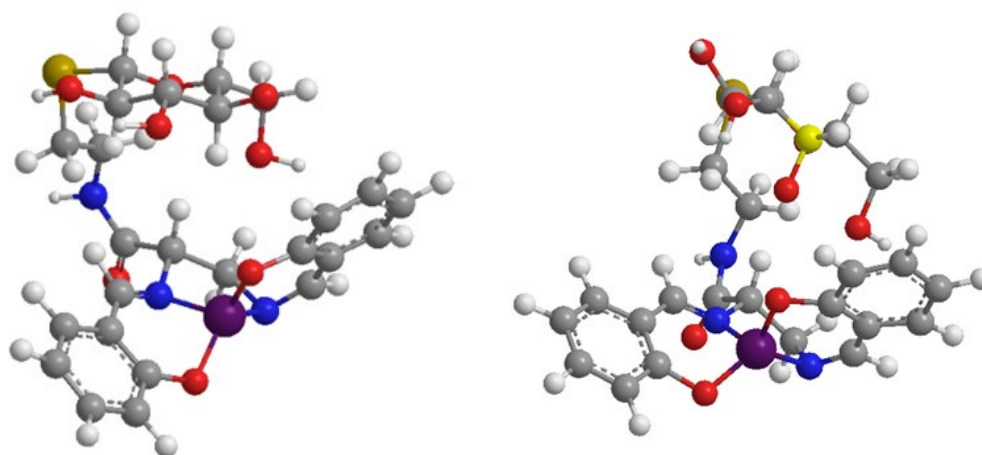


Figure 3. Molecular modelling of **4a** (left) and **4b** (right).

**4a** and **4b** activities were also investigated in the presence of RCA<sub>120</sub>. The **4a**/ or **4b**/RCA<sub>120</sub> adducts were synthesized by pre-incubating equimolar amounts of RCA<sub>120</sub> lectin and **4a** or **4b** for 15 min in the buffer solution at 25 °C.

The RCA<sub>120</sub> alone did not show any interference with the SOD assay. The  $I_{50}$  value of the **4a**–RCA<sub>120</sub> adduct was  $5.0 \times 10^{-8} \text{ M}$  and the  $k_{cat}$  was  $2.8 \times 10^8 \text{ M}^{-1} \text{ s}^{-1}$  (Table 1, Figure S15). These values were significantly higher than those of the free **4b** and they were of the same order of magnitude as that of the native SOD1 enzyme ( $1.4 \times 10^8 \text{ M}$ ) [52]. No activity improvement was observed when **4b** was pre-incubated with RCA120 [8].

Table 1. SOD-like activity in the Fridovich assay (NBT = 250 μM) of **4a**, **4b**, and their RCA<sub>120</sub> adducts.

Complex	$I_{50}$ (μM)	$k_{cat}$ (M <sup>-1</sup> s <sup>-1</sup> )
EUK-108	2.05 (±0.03)	$(7.2 \pm 0.9) \times 10^6$
<b>4a</b>	0.20 (±0.04)	$(7.4 \pm 0.7) \times 10^7$
<b>4b</b>	0.25 (±0.05)	$(5.9 \pm 0.4) \times 10^7$
<b>4a</b> /RCA <sub>120</sub>	0.05 (±0.01)	$(2.9 \pm 0.3) \times 10^8$
<b>4b</b> /RCA <sub>120</sub>	0.20 (±0.03)	$(8.0 \pm 0.4) \times 10^7$

We hypothesized that RCA<sub>120</sub> could bind **4a**, as reported for other galactose conjugates [35,53], and that the protein environment could modulate the activity of the catalytic center, as found for other SOD-mimetic hybrid systems [39,54–56]. The interaction between the RCA<sub>120</sub> and **4a** complex was investigated using CD spectroscopy. In the UV region of the CD spectra (Figure S16), RCA<sub>120</sub> showed a positive peak at 190 nm and negative peaks at 208 nm and 220 nm, in keeping with the partial  $\alpha$ -helix structure of RCA<sub>120</sub> (15%) [53]. The intensity of the signals was slightly modified after the addition of the **4a** complex to RCA<sub>120</sub> (Figure S16), suggesting the interaction of **4a** with the protein. No modification of the CD spectrum of RCA<sub>120</sub> was found when **4b** was added to RCA<sub>120</sub> (Figure S17). These data can explain the effect on the SOD activity in the presence of the RCA<sub>120</sub> protein, which can only bind the **4a** complex.

### 3.4. Catalase Activity

Both salen complexes **4a** and **4b** exhibited a similar catalase activity, and their activities (Table 2) were slightly lower than EUK-108's [45].

**Table 2.** Catalase and peroxidase activity of **4a**, **4b**, and their RCA<sub>120</sub> adducts.

Complex	CAT Activity	Peroxidase Activity
	$\mu\text{mol H}_2\text{O}_2/\text{min}/\text{mmol}$	$\mu\text{M ABTS}/\text{min}$
EUK108	32.2 ( $\pm 1.7$ )	18.3 ( $\pm 0.7$ )
<b>4a</b>	40.8 ( $\pm 1.5$ )	21.6 ( $\pm 0.6$ )
<b>4b</b>	40.6 ( $\pm 1.2$ )	23.3 ( $\pm 0.5$ )
<b>4a/RCA<sub>120</sub></b>	31.5 ( $\pm 1.5$ )	35.7 ( $\pm 0.7$ )
<b>4b/RCA<sub>120</sub></b>	28.8 ( $\pm 1.2$ )	25.3 ( $\pm 1.0$ )

The reaction mechanism by which the Mn complexes act as catalase mimetics has been investigated [45]. It involves the oxidation of Mn<sup>III</sup> by H<sub>2</sub>O<sub>2</sub> to oxo-manganese and the formation of H<sub>2</sub>O. The oxo-manganese complex is then reduced to Mn<sup>III</sup> by another H<sub>2</sub>O<sub>2</sub> molecule to form O<sub>2</sub>.

The presence of RCA<sub>120</sub> slightly changed the CAT activity of both complexes.

### 3.5. Peroxidase Activity

The peroxidase activities of **4a**, **4b**, and EUK-108 were determined using the ABTS assay [29,30,34]. ABTS was the model substrate which reacted with H<sub>2</sub>O<sub>2</sub>



Mn complexes can catalyze the oxidation of ABTS with H<sub>2</sub>O<sub>2</sub> (peroxidase activity). The mechanism for salen-Mn<sup>III</sup> complexes consisted in the formation of the oxo-manganese complex intermediate, which could oxidate the ABTS generating ABTS<sup>·+</sup>. [57–60].

The UV-vis spectrum of the green ABTS<sup>·+</sup> radical cation showed characteristic bands at 415, 650, 735, and 815 nm. The solution of ABTS and H<sub>2</sub>O<sub>2</sub> without the Mn complex was stable for several hours at 25 °C [33].

The amount of the ABTS<sup>·+</sup> formed per minute ( $\mu\text{M ABTS}/\text{min}$ ) at the concentration of the complex  $1.0 \times 10^{-5}$  M is reported in Table 2.

The two Mn<sup>III</sup> glycosalen complexes showed similar peroxidase activity compared to EUK-108.

The RCA<sub>120</sub>-**4a** adduct slightly improved the peroxidase activity compared to **4a** (Table 2). No effect of RCA<sub>120</sub> was found for **4b**.

## 4. Conclusions

Antioxidant enzymes play a crucial role in physiological and pathological states. SOD mimetics may provide therapeutic strategies in redox medicine to reduce the severity of

diseases related to oxidative stress. A family of SOD/Catalase mimetics are Mn<sup>III</sup> complexes of salen-type ligands.

We synthesized new glycoconjugates of EUK-108 and their Mn<sup>III</sup> complexes. The sugar moiety increased the solubility in the water of the system compared to that of the free EUK-108. The glycoconjugation improved the efficiency of SOD mimetics by about ten times compared to that of the free EUK-108. Instead, the glycoconjugates showed a similar catalase and peroxidase activity to the EUK-108. The sugar moiety conferred new properties to the conjugates, such as the binding with specific lectins. We found that the galactose derivative interacted with RCA<sub>120</sub> lectin, which can selectively recognize galactose units. The hybrid system galactose–EUK-108–RCA<sub>120</sub> lectin showed five times better SOD-like activity compared to that of the free galactose–EUK-108 conjugate. The hybrid system showed a SOD activity similar to that of the native SOD1 enzyme. The RCA<sub>120</sub> protein environment could modulate the activity of the catalytic center.

These results disclose the potential of supramolecular mimetics. Based on the interest in antioxidant enzyme mimetics to counteract oxidative stress, this approach could be helpful for further improvement of the SOD mimetics.

**Supplementary Materials:** The following supporting information can be downloaded at: <https://www.mdpi.com/article/10.3390/biomimetics8050447/s1>, Figures S1–S13: NMR and ESI spectra; Figures S14 and S15: SOD-like activity; Figures S16–S17: CD spectra of RCA<sub>120</sub>.

**Author Contributions:** All the authors were involved in conceptualization, methodology, investigation, resources, data curation, writing and editing. All authors have read and agreed to the published version of the manuscript.

**Funding:** The authors acknowledge support from Università degli Studi di Catania (Piano di incentivi per la ricerca di Ateneo 2020/2022 (Pia.ce.ri)).

**Institutional Review Board Statement:** Not applicable.

**Data Availability Statement:** The authors confirm that the data supporting the findings of this study are available within the article and its supplementary materials.

**Conflicts of Interest:** The authors declare no conflict of interest.

## References

1. Chatterjee, S. Chapter two—Oxidative stress, inflammation, and disease. In *Oxidative Stress and Biomaterials*; Dziubla, T., Butterfield, D.A., Eds.; Academic Press: Cambridge, MA, USA, 2016; pp. 35–58. ISBN 978-0-12-803269-5.
2. Ramos-González, E.J.; Bitzer-Quintero, O.K.; Ortiz, G.; Hernández-Cruz, J.J.; Ramírez-Jirano, L.J. Relationship between inflammation and oxidative stress and its effect on multiple sclerosis. *Neurología* **2021**, in press. [CrossRef]
3. He, L.; He, T.; Farrar, S.; Ji, L.; Liu, T.; Ma, X. Antioxidants Maintain Cellular Redox Homeostasis by Elimination of Reactive Oxygen Species. *Cell. Physiol. Biochem.* **2017**, *44*, 532–553. [CrossRef] [PubMed]
4. Sies, H.; Jones, D.P. Reactive Oxygen Species (ROS) as Pleiotropic Physiological Signalling Agents. *Nat. Rev. Mol. Cell Biol.* **2020**, *21*, 363–383. [CrossRef] [PubMed]
5. Forman, H.J.; Zhang, H. Targeting Oxidative Stress in Disease: Promise and Limitations of Antioxidant Therapy. *Nat. Rev. Drug Discov.* **2021**, *20*, 689–709. [CrossRef] [PubMed]
6. McIlwain, H.; Silverfield, J.C.; Cheatum, D.E.; Poiley, J.; Taborn, J.; Ignaczak, T.; Multz, C.V. Intra-Articular Orgotein in Osteoarthritis of the Knee: A Placebo-Controlled Efficacy, Safety, and Dosage Comparison. *Am. J. Med.* **1989**, *87*, 295–300. [CrossRef] [PubMed]
7. Bonetta, R. Potential Therapeutic Applications of MnSODs and SOD-Mimetics. *Chem. Eur. J.* **2018**, *24*, 5032–5041. [CrossRef] [PubMed]
8. Batinic-Haberle, I.; Tovmasyan, A.; Roberts, E.R.H.; Vujaskovic, Z.; Leong, K.W.; Spasojevic, I. SOD Therapeutics: Latest Insights into Their Structure-Activity Relationships and Impact on the Cellular Redox-Based Signaling Pathways. *Antioxid. Redox Signal.* **2014**, *20*, 2372–2415. [CrossRef]
9. Bigham, N.P.; Wilson, J.J. Metal Coordination Complexes as Therapeutic Agents for Ischemia-Reperfusion Injury. *J. Am. Chem. Soc.* **2023**, *145*, 9389–9409. [CrossRef]
10. Policar, C.; Bouvet, J.; Bertrand, H.C.; Delsuc, N. SOD Mimics: From the Tool Box of the Chemists to Cellular Studies. *Curr. Opin. Chem. Biol.* **2022**, *67*, 102109. [CrossRef]
11. Rosenthal, R.; Fish, B.; Hill, R.P.; Huffman, K.; Lazarova, Z.; Mahmood, J.; Medhora, M.; Molthen, R.; Moulder, J.E.; Sonis, S.; et al. Salen Mn Complexes Mitigate Radiation Injury in Normal Tissues. *Anticancer Agents Med. Chem.* **2011**, *11*, 359–372. [CrossRef]

12. Karlsson, J.O.G.; Jynge, P.; Ignarro, L.J. May Mangafodipir or Other SOD Mimetics Contribute to Better Care in COVID-19 Patients? *Antioxid. Basel Switz.* **2020**, *9*, 971. [[CrossRef](#)] [[PubMed](#)]
13. Liu, M.; Sun, X.; Chen, B.; Dai, R.; Xi, Z.; Xu, H. Insights into Manganese Superoxide Dismutase and Human Diseases. *Int. J. Mol. Sci.* **2022**, *23*, 15893. [[CrossRef](#)] [[PubMed](#)]
14. Miriyala, S.; Spasojevic, I.; Tovmasyan, A.; Salvemini, D.; Vujaskovic, Z.; Clair, D.S.; Batinic-Haberle, I. Manganese Superoxide Dismutase, MnSOD and Its Mimics. *Biochim. Biophys. Acta* **2012**, *1822*, 794–814. [[CrossRef](#)]
15. Vincent, A.; Thauvin, M.; Quévrain, E.; Mathieu, E.; Layani, S.; Seksik, P.; Batinic-Haberle, I.; Vriza, S.; Policar, C.; Delsuc, N. Evaluation of the Compounds Commonly Known as Superoxide Dismutase and Catalase Mimics in Cellular Models. *J. Inorg. Biochem.* **2021**, *219*, 111431. [[CrossRef](#)] [[PubMed](#)]
16. Mapuskar, K.A.; Vasquez Martinez, G.; Pulliam, C.F.; Petronek, M.S.; Steinbach, E.J.; Monga, V.; Furqan, M.; Jetton, J.G.; Saunders, D.P.; Pearce, A.; et al. Avasopasem Manganese (GC4419) Protects against Cisplatin-Induced Chronic Kidney Disease: An Exploratory Analysis of Renal Metrics from a Randomized Phase 2b Clinical Trial in Head and Neck Cancer Patients. *Redox Biol.* **2023**, *60*, 102599. [[CrossRef](#)] [[PubMed](#)]
17. Anderson, C.M.; Lee, C.M.; Saunders, D.P.; Curtis, A.; Dunlap, N.; Nangia, C.; Lee, A.S.; Gordon, S.M.; Kovoor, P.; Arevalo-Araujo, R.; et al. Phase IIb, Randomized, Double-Blind Trial of GC4419 Versus Placebo to Reduce Severe Oral Mucositis Due to Concurrent Radiotherapy and Cisplatin For Head and Neck Cancer. *J. Clin. Oncol. Off. J. Am. Soc. Clin. Oncol.* **2019**, *37*, 3256–3265. [[CrossRef](#)] [[PubMed](#)]
18. Galera Therapeutics, Inc. A Pilot, Randomized, Placebo-Controlled Trial of GC4419 (Avasopasem Manganese) in Patients with Critical Illness Due to SARS-CoV-2 Infection (COVID-19). 2022. Available online: [Clinicaltrials.gov](https://clinicaltrials.gov) (accessed on 7 July 2023).
19. Mathieu, E.; Bernard, A.-S.; Ching, H.Y.V.; Somogyi, A.; Medjoubi, K.; Fores, J.R.; Bertrand, H.C.; Vincent, A.; Trépout, S.; Guerquin-Kern, J.-L.; et al. Anti-Inflammatory Activity of Superoxide Dismutase Mimics Functionalized with Cell-Penetrating Peptides. *Dalton Trans.* **2020**, *49*, 2323–2330. [[CrossRef](#)]
20. Batinic-Haberle, I.; Tovmasyan, A.; Spasojevic, I. An Educational Overview of the Chemistry, Biochemistry and Therapeutic Aspects of Mn Porphyrins—From Superoxide Dismutation to H<sub>2</sub>O<sub>2</sub>-Driven Pathways. *Redox Biol.* **2015**, *5*, 43–65. [[CrossRef](#)]
21. Signorella, S.; Palopoli, C.; Ledesma, G. Rationally Designed Mimics of Antioxidant Manganoenzymes: Role of Structural Features in the Quest for Catalysts with Catalase and Superoxide Dismutase Activity. *Coord. Chem. Rev.* **2018**, *365*, 75–102. [[CrossRef](#)]
22. Batinic-Haberle, I.; Tovmasyan, A.; Huang, Z.; Duan, W.; Du, L.; Siamakpour-Reihani, S.; Cao, Z.; Sheng, H.; Spasojevic, I.; Alvarez Secord, A. H<sub>2</sub>O<sub>2</sub>-Driven Anticancer Activity of Mn Porphyrins and the Underlying Molecular Pathways. *Oxid. Med. Cell. Longev.* **2021**, *2021*, 6653790. [[CrossRef](#)]
23. Olson, K.R.; Gao, Y.; Arif, F.; Patel, S.; Yuan, X.; Mannam, V.; Howard, S.; Batinic-Haberle, I.; Fukuto, J.; Minnion, M.; et al. Manganese Porphyrin-Based SOD Mimetics Produce Polysulfides from Hydrogen Sulfide. *Antioxidants* **2019**, *8*, 639. [[CrossRef](#)] [[PubMed](#)]
24. Doctrow, S.R.; Fish, B.; Huffman, K.D.; Lazarova, Z.; Medhora, M.; Williams, J.P.; Moulder, J.E. Salen Manganese Complexes Mitigate Radiation Injury in Normal Tissues Through Modulation of Tissue Environment, Including Through Redox Mechanisms. In *Redox-Active Therapeutics*; Batinić-Haberle, I., Rebouças, J.S., Spasojević, I., Eds.; Oxidative Stress in Applied Basic Research and Clinical Practice; Springer International Publishing: Cham, Switzerland, 2016; pp. 265–285. ISBN 978-3-319-30705-3.
25. Rouco, L.; González-Noya, A.M.; Pedrido, R.; Maneiro, M. Pursuing the Elixir of Life: In Vivo Antioxidative Effects of Manganosalen Complexes. *Antioxidants* **2020**, *9*, 727. [[CrossRef](#)] [[PubMed](#)]
26. Noritake, Y.; Umezawa, N.; Kato, N.; Higuchi, T. Manganese Salen Complexes with Acid–Base Catalytic Auxiliary: Functional Mimetics of Catalase. *Inorg. Chem.* **2013**, *52*, 3653–3662. [[CrossRef](#)] [[PubMed](#)]
27. McDonald, M.C.; d’Emmanuele di Villa Bianca, R.; Wayman, N.S.; Pinto, A.; Sharpe, M.A.; Cuzzocrea, S.; Chatterjee, P.K.; Thiemermann, C. A Superoxide Dismutase Mimetic with Catalase Activity (EUK-8) Reduces the Organ Injury in Endotoxic Shock. *Eur. J. Pharmacol.* **2003**, *466*, 181–189. [[CrossRef](#)] [[PubMed](#)]
28. Himori, K.; Abe, M.; Tatebayashi, D.; Lee, J.; Westerblad, H.; Lanner, J.T.; Yamada, T. Superoxide Dismutase/Catalase Mimetic EUK-134 Prevents Diaphragm Muscle Weakness in Monocrotalin-Induced Pulmonary Hypertension. *PLoS ONE* **2017**, *12*, e0169146. [[CrossRef](#)] [[PubMed](#)]
29. Menezes, L.B.; Segat, B.B.; Tolentino, H.; Pires, D.C.; Mattos, L.M.D.M.; Hottum, H.M.; Pereira, M.D.; Latini, A.; Horn, A.J.; Fernandes, C. ROS Scavenging of SOD/CAT Mimics Probed by EPR and Reduction of Lipid Peroxidation in *S. Cerevisiae* and Mouse Liver, under Severe Hydroxyl Radical Stress Condition. *J. Inorg. Biochem.* **2023**, *239*, 112062. [[CrossRef](#)] [[PubMed](#)]
30. Segat, B.B.; Menezes, L.B.; Cervo, R.; Cargnelutti, R.; Tolentino, H.; Latini, A.; Horn, A.J.; Fernandes, C. Scavenging of Reactive Species Probed by EPR and Ex-Vivo Nanomolar Reduction of Lipid Peroxidation of Manganese Complexes. *J. Inorg. Biochem.* **2023**, *239*, 112060. [[CrossRef](#)]
31. Ning, Y.; Huo, Y.; Xue, H.; Du, Y.; Yao, Y.; Sedgwick, A.C.; Lin, H.; Li, C.; Jiang, S.-D.; Wang, B.-W.; et al. Tri-Manganese(III) Salen-Based Cryptands: A Metal Cooperative Antioxidant Strategy That Overcomes Ischemic Stroke Damage in Vivo. *J. Am. Chem. Soc.* **2020**, *142*, 10219–10227. [[CrossRef](#)]
32. Rouco, L.; Alvaríño, R.; Alfonso, A.; Romero, M.J.; Pedrido, R.; Maneiro, M. Neuroprotective Effects of Fluorophore-Labelled Manganese Complexes: Determination of ROS Production, Mitochondrial Membrane Potential and Confocal Fluorescence Microscopy Studies in Neuroblastoma Cells. *J. Inorg. Biochem.* **2022**, *227*, 111670. [[CrossRef](#)]

33. Doctrow, S.R.; Huffman, K.; Marcus, C.B.; Musleh, W.; Bruce, A.; Baudry, M.; Malfroy, B. Salen-Manganese Complexes: Combined Superoxide Dismutase/Catalase Mimics with Broad Pharmacological Efficacy. *Adv. Pharmacol.* **1996**, *38*, 247–269.
34. Puglisi, A.; Tabbi, G.; Vecchio, G. Bioconjugates of Cyclodextrins of Manganese Salen-Type Ligand with Superoxide Dismutase Activity. *J. Inorg. Biochem.* **2004**, *98*, 969–976. [[CrossRef](#)] [[PubMed](#)]
35. Lanza, V.; D'Agata, R.; Iacono, G.; Bellia, F.; Spoto, G.; Vecchio, G. Cyclam Glycoconjugates as Lectin Ligands and Protective Agents of Metal-Induced Amyloid Aggregation. *J. Inorg. Biochem.* **2015**, *153*, 377–382. [[CrossRef](#)] [[PubMed](#)]
36. Maljaars, C.E.P.; Halkes, K.M.; De Oude, W.L.; Haseley, S.R.; Upton, P.J.; McDonnell, M.B.; Kamerling, J.P. Affinity Determination of *Ricinus communis* Agglutinin Ligands Identified from Combinatorial O- and S-, N-Glycopeptide Libraries. *J. Comb. Chem.* **2006**, *8*, 812–819. [[CrossRef](#)] [[PubMed](#)]
37. Hanreich, S.; Bonandi, E.; Drienovská, I. Design of Artificial Enzymes: Insights into Protein Scaffolds. *ChemBioChem* **2023**, *24*, e202200566. [[CrossRef](#)] [[PubMed](#)]
38. Davis, H.J.; Ward, T.R. Artificial Metalloenzymes: Challenges and Opportunities. *ACS Cent. Sci.* **2019**, *5*, 1120–1136. [[CrossRef](#)] [[PubMed](#)]
39. Yang, X.; Wu, W.; Chen, X.; Wu, F.; Fan, S.; Yu, P.; Mao, L. A Versatile Artificial Metalloenzyme Scaffold Enabling Direct Bioelectrocatalysis in Solution. *Sci. Adv.* **2022**, *8*, eabo3315. [[CrossRef](#)] [[PubMed](#)]
40. DiPrimio, D.J.; Holland, P.L. Repurposing Metalloproteins as Mimics of Natural Metalloenzymes for Small-Molecule Activation. *J. Inorg. Biochem.* **2021**, *219*, 111430. [[CrossRef](#)]
41. Jeschek, M.; Reuter, R.; Heinisch, T.; Trindler, C.; Klehr, J.; Panke, S.; Ward, T.R. Directed Evolution of Artificial Metalloenzymes for in Vivo Metathesis. *Nature* **2016**, *537*, 661–665. [[CrossRef](#)]
42. Haikarainen, A.; Sipilä, J.; Pietikäinen, P.; Pajunen, A.; Mutikainen, I. Synthesis and Characterization of Bulky Salen-Type Complexes of Co, Cu, Fe, Mn and Ni with Amphiphilic Solubility Properties. *J. Chem. Soc. Dalton Trans.* **2001**, *7*, 991–995. [[CrossRef](#)]
43. Beauchamp, C.; Fridovich, I. Superoxide Dismutase: Improved Assays and an Assay Applicable to Acrylamide Gels. *Anal. Biochem.* **1971**, *44*, 276–287. [[CrossRef](#)]
44. Lanza, V.; Vecchio, G. New Conjugates of Superoxide Dismutase/Catalase Mimetics with Cyclodextrins. *J. Inorg. Biochem.* **2009**, *103*, 381–388. [[CrossRef](#)] [[PubMed](#)]
45. Doctrow, S.R.; Huffman, K.; Marcus, C.B.; Tocco, G.; Malfroy, E.; Adinolfi, C.A.; Kruk, H.; Baker, K.; Lazarowych, N.; Mascarenhas, J.; et al. Salen–Manganese Complexes as Catalytic Scavengers of Hydrogen Peroxide and Cytoprotective Agents: Structure–Activity Relationship Studies. *J. Med. Chem.* **2002**, *45*, 4549–4558. [[CrossRef](#)] [[PubMed](#)]
46. Gonzalez, P.K.; Zhuang, J.; Doctrow, S.R.; Malfroy, B.; Benson, P.F.; Menconi, M.J.; Fink, M.P. EUK-8, a Synthetic Superoxide Dismutase and Catalase Mimetic, Ameliorates Acute Lung Injury in Endotoxemic Swine. *J. Pharmacol. Exp. Ther.* **1995**, *275*, 798–806. [[PubMed](#)]
47. Zhao, H.; Zhang, R.; Yan, X.; Fan, K. Superoxide Dismutase Nanozymes: An Emerging Star for Anti-Oxidation. *J. Mater. Chem. B* **2021**, *9*, 6939–6957. [[CrossRef](#)] [[PubMed](#)]
48. Senthilkumar, M.; Amaesan, N.; Sankaranarayanan, A. (Eds.) Estimation of Superoxide Dismutase (SOD). In *Plant-Microbe Interactions: Laboratory Techniques*; Springer Protocols Handbooks; Springer US: New York, NY, USA, 2021; pp. 117–118. ISBN 978-1-07-161080-0.
49. Durot, S.; Policar, C.; Cisnetti, F.; Lambert, F.; Renault, J.-P.; Pelosi, G.; Blain, G.; Korri-Youssoufi, H.; Mahy, J.-P. Series of Mn Complexes Based on N-Centered Ligands and Superoxide—Reactivity in an Anhydrous Medium and SOD-Like Activity in an Aqueous Medium Correlated to MnII/MnIII Redox Potentials. *Eur. J. Inorg. Chem.* **2005**, *2005*, 3513–3523. [[CrossRef](#)]
50. Bielski, B.H.J.; Shiue, G.G.; Bajuk, S. Reduction of Nitro Blue Tetrazolium by CO<sub>2</sub>- and O<sub>2</sub>- Radicals. *J. Phys. Chem.* **1980**, *84*, 830–833. [[CrossRef](#)]
51. Shaw, S.; White, J.D. Asymmetric Catalysis Using Chiral Salen–Metal Complexes: Recent Advances. *Chem. Rev.* **2019**, *119*, 9381–9426. [[CrossRef](#)]
52. Bonomo, R.P.; Bruno, V.; Conte, E.; De Guidi, G.; La Mendola, D.; Maccarrone, G.; Nicoletti, F.; Rizzarelli, E.; Sortino, S.; Vecchio, G. Potentiometric, Spectroscopic and Antioxidant Activity Studies of SOD Mimics Containing Carnosine. *J. Chem. Soc. Dalton Trans.* **2003**, *3*, 4406–4415. [[CrossRef](#)]
53. Shimazaki, K.; Walborg, E.F.; Neri, G.; Jirgensons, B. Circular Dichroism and Saccharide-Induced Conformational Transitions of Lectins from *Ricinus Communis*. *Arch. Biochem. Biophys.* **1975**, *169*, 731–736. [[CrossRef](#)]
54. Xu, Z.; Pan, S.; Li, G.; He, Y.-F.; Wang, R. Albumin Conjugating Amino Acid Schiff-Base Metal Complexes for Scavenging Superoxide Anion Radical. *J. Inorg. Organomet. Polym. Mater.* **2015**, *25*, 1313–1319. [[CrossRef](#)]
55. Oliveri, V.; Vecchio, G. A Novel Artificial Superoxide Dismutase: Non-Covalent Conjugation of Albumin with a MnIIIsalophen Type Complex. *Eur. J. Med. Chem.* **2011**, *46*, 961–965. [[CrossRef](#)] [[PubMed](#)]
56. Furuya, T.; Nakane, D.; Kitanishi, K.; Katsuumi, N.; Tsaturyan, A.; Shcherbakov, I.N.; Unno, M.; Akitsu, T. A Novel Hybrid Protein Composed of Superoxide-Dismutase-Active Cu(II) Complex and Lysozyme. *Sci. Rep.* **2023**, *13*, 6892. [[CrossRef](#)] [[PubMed](#)]
57. Kim, M.-C.; Lee, S.-Y. Peroxidase-like Oxidative Activity of a Manganese-Coordinated Histidyl Bolaamphiphile Self-Assembly. *Nanoscale* **2015**, *7*, 17063–17070. [[CrossRef](#)]

58. Bermejo, M.R.; Fernández, M.I.; González-Noya, A.M.; Maneiro, M.; Pedrido, R.; Rodríguez, M.J.; García-Monteagudo, J.C.; Donnadieu, B. Novel Peroxidase Mimics:  $\mu$ -Aqua Manganese–Schiff Base Dimers. *J. Inorg. Biochem.* **2006**, *100*, 1470–1478. [[CrossRef](#)] [[PubMed](#)]
59. Moreno-Castilla, C.; Naranjo, Á.; Victoria López-Ramón, M.; Siles, E.; López-Peñalver, J.J.; de Almodóvar, J.M.R. Influence of the Hydrodynamic Size and  $\zeta$  Potential of Manganese Ferrite Nanozymes as Peroxidase-Mimicking Catalysts at pH 4 in Different Buffers. *J. Catal.* **2022**, *414*, 179–185. [[CrossRef](#)]
60. Liberato, A.; Fernández-Trujillo, M.J.; Mániz, Á.; Maneiro, M.; Rodríguez-Silva, L.; Basallote, M.G. Pitfalls in the ABTS Peroxidase Activity Test: Interference of Photochemical Processes. *Inorg. Chem.* **2018**, *57*, 14471–14475. [[CrossRef](#)]

**Disclaimer/Publisher’s Note:** The statements, opinions and data contained in all publications are solely those of the individual author(s) and contributor(s) and not of MDPI and/or the editor(s). MDPI and/or the editor(s) disclaim responsibility for any injury to people or property resulting from any ideas, methods, instructions or products referred to in the content.